Exploring the effects of interfacial carrier transport layers on device performance and optoelectronic properties of planar perovskite solar cells

Dhruba B. Khadka,[†]* Yasuhiro Shirai,[†]* Masatoshi Yanagida,[†] James W. Ryan,[†‡] and Kenjiro Miyano[†]

[†] Global Research Center for Environment and Energy based on Nanomaterials Science (GREEN), National Institute for Materials Science (NIMS), 1-1 Namiki, Tsukuba, Ibaraki 305-0044, Japan.

[‡] International Center for Young Scientists (ICYS), National Institute for Materials Science (NIMS), 1-1 Namiki, Tsukuba, Ibaraki 305-0044, Japan.

Corresponding Authors

*E-mail:

KHADKA.B.Dhruba@nims.go.jp

SHIRAI.Yasuhiro@nims.go.jp

Abstract

We investigated the effects of carrier transport layer on performance of perovskite device and limitation factors by analysing the optoelectronic properties. The device efficiency was enhanced from ~14.5% to ~18.1% by replacing hole transport layer (HTL) PEDOT:PSS with PTAA, governed by increase in open circuit voltage and short circuit current. We found that PTAA device leads to the improvement in interface layer quality, efficient carrier transport and mitigation of bulk defect activities. The analysis of temperature and intensity dependent current-voltage characteristics suggests that PEDOT:PSS device is limited by interface and trap assisted recombination. The capacitance spectroscopy and electroluminescence revealed soothing of recombination activities as a consequence of better interface quality and shallower defect level for PTAA device. Our results consolidate that the perovskite film and interface quality and recombination activities in device are dominantly influenced by HTLs which pave a way for further enhancement in efficiency coupled with excellent interfacial carrier transport layer.

Keywords: Perovskite, carrier transport, defect state, interface quality, recombination

Introduction

Lead halide perovskite solar cells have made rapid progress since the independent reports of Snaith and Park in 2012, where they demonstrated the first solid state perovskite solar cells with efficiencies ~10%.[1,2] Since then, device efficiencies have more than doubled, with the current record standing at ~22% for a single junction device.[3] Such a rapid advance in performance in the space of five years is unprecedented in photovoltaics, particularly for solar cells based on solution-processed semiconductors. The reason for the high performance of lead halide perovskite solar cells stems from the excellent optoelectronic properties (high absorption coefficient, high charge carrier mobility, long diffusion lengths) and the ability to deposit highly crystalline and uniform thin films.[4–6] Indeed, there now exists a plethora of approaches for preparing high quality perovskite thin films via solution processing and interface engineering of the device with carrier transport layers for effective carrier extraction.[7–13] However, a common problem faced by many researchers in preparing high performance perovskite solar cells comes from the choice of charge transport layers (CTLs) in order to extract all the photogenerated charge carriers from the perovskite layer while avoiding carrier recombination. The CTLs are crucial to overcome the hysteresis and stability of devices and also equally important to facilitate larger grain and better crystallinity of perovskite layer.[9,14–16]

A number of efforts have been made to achieve better performance of perovskite solar cells (PVSCs) by engineering the organic/inorganic materials as hole/electron transport layer (HTL/ETL).[6,11–13,17–19] An added problem that depends on the interfacial layers is photocurrent hysteresis. Although its origin is not fully understood till date, the photocurrent hysteresis issue has been eliminated by sandwiching the perovskite layer with proper selection of CTLs.[15,20] The hysteresis observed in perovskite device has been illustrated with mechanism considering ion migration process during J-V scan, induced ferroelectric

properties under bias and trapping/de-trapping of carriers at the interface and bulk of perovskite layer.[20–24] Despite the improvement in device performance with selective CTLs leading to enhancement in open circuit voltage (V_{OC}),[13–15,17–19] there are few reports dealing the phenomena behind it.[24–28] The perovskite devices with PEDOT:PSS as HTL have shown hysteresis free and high reproducibility but the device performances are limited by lower V_{OC} (below 1 V).[11,14,29,30] Understanding the loss processes that limit V_{OC} is imperative to developing record efficiencies for perovskite solar cells. The choice of HTL is vital for removing interfacial loss processes.[25,26,28] Heo et al.[17] have reported an enhancement in perovskite device efficiencies employing various polymeric hole transport materials. Ryu et al.[18] demonstrated the efficient PVSCs with high V_{OC} and fill factor by tuning the HOMO level of HTLs. Liu et al. observed that the nonreduction active hole transport layer is crucial to passivate a chemical reaction during processing of perovskite film on HTL and consequently increase in V_{OC} and efficiencies of inverted planar PVSCs.[29] Huang and co-workers[11,14] reported that the wetting property of HTLs promote larger grains with high quality perovskite film and hence improvement in device performances. Xu et al.[31] demonstrated an enhancement in device efficiency employing an ultra-violet ozone modification on non-wetting HTLs benefiting with high quality perovskite film. Only few of reports have investigated the factors affecting the device performance in optoelectronic approach. Brabec and co-workers reported an analysis of the loss mechanism unveiling some facts behind the interface loss and V_{OC} limitation in planar perovskite solar cells.[25,26] Shao et al.[10] investigated correlation of energy disorder in transport layers and V_{OC} in perovskite device. Despite some reports on the temperature dependent photovoltaic performance of perovskite devices,[28,32–35] there is still lack of comparative study and lucid argument following the temperature dependent device characteristics. Indeed, systematic investigations on recombination phenomena at interface or in bulk defects in perovskite layer impacted by

the CTLs are necessary to enrich understanding on loss mechanism. This will provide a solid foundation to develop a strategy for further progress in device efficiency.

Here, we report on a quantitative analysis of enhancement of device efficiency of perovskite solar cell fabricated by replacing customarily used hole transport material, PEDOT:PSS in our earlier reports[20,30,36] with PTAA which permits higher V_{OC} leading to an enhancement in device performance from ~14.5% to 18.1%. We employed a series of experiments to gain a clear understanding on the role of the HTL and the factors limiting PEDOT:PSS based devices. We investigated the temperature dependent current-voltage (J-V) characteristics, capacitance spectroscopy and biased spectral response of those devices to understand the phenomena behind the enhancement in power conversion efficiency (PCE). A detailed analysis on device characteristics in optoelectronic approach revealed that the PTAA device has a reduced recombination at PTAA/perovskite interface, mitigates the defect states and passivates defect activities as a consequence of better interface quality and improved crystallinity of perovskite layer. Time-resolved photoluminescence and steady-state electroluminescence offer additional information on the quality of the HTL/perovskite interface and carrier transfer. We have carried out the device simulation using SCAPS (solar cell capacitor simulator) mimicking the experimental results to support our interpretation.

Results and discussion

Planar heterojunction perovskite solar cells were fabricated with the following configuration: ITO/HTL/$CH_3NH_3PbI_{3-x}Cl_x$/PCBM/AZO/Ag as depicted in **Fig. 1a**. We prepared perovskite devices with PEDOT:PSS or PTAA as HTL and perovskite layers sandwiched with PCBM as ETL along with a thin semiconducting layer of Al:ZnO (AZO) as an electron selective layer (ESL) beneath the Ag electrode. AZO used here is also found to be well working which is

beneficial for deposition of transparent conductor oxide (TCO) layer as electrode for transparent or tandem perovskite devices.[37,38] **Fig. 1b** illustrates the energy band diagram.

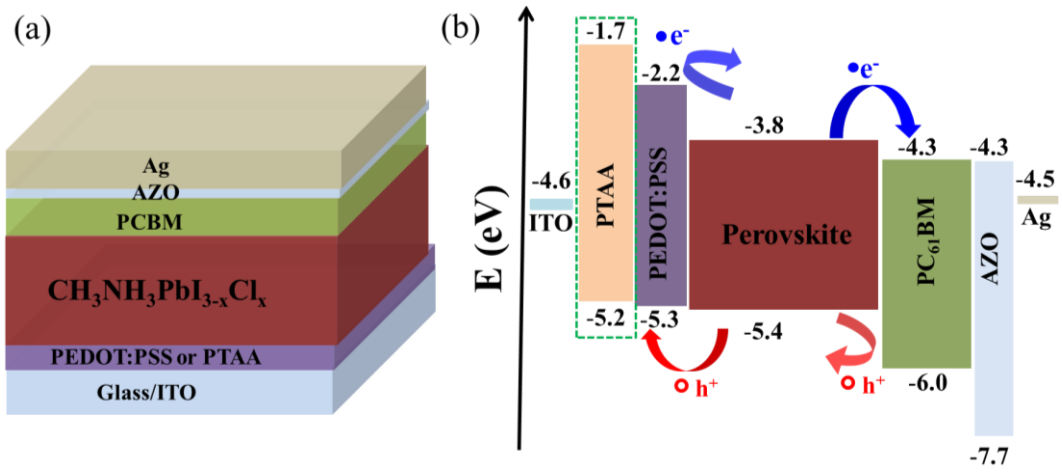

Fig. 1. Device structure of the perovskite planar heterojunction solar cells: ITO/HTL/ Perovskite/PCBM/AZO/Ag (a). Schematic of the energy band diagrams for all materials employed (b) estimated by photoelectron spectroscopy. Enclosed dot line represents replaced HTL (PTAA).

Figure 2a shows the J-V curves of perovskite devices fabricated with PEDOT:PSS and PTAA as HTLs, measured at room temperature under standard one sun illumination conditions (AM 1.5G, 100 $mWcm^{-2}$). The figures of merit for each device are presented in **Table 1.** A significant increase in PCE is observed for PTAA devices, 18.1%, compared to PEDOT:PSS devices, 14.5%. The improved device efficiency stems from a significant increase in V_{OC} (from 0.95 to 1.09 V) as well as an increase in J_{SC} (19.7 to 21.0 $mAcm^{-2}$) (**Fig. 2a, Fig. S1**). These trends were found to be reproducible for a large set of devices, as summarized in the supporting information (**Fig. S1**, **Table S1**). Despite PEDOT:PSS having a higher ionization potential, it does not enhance V_{OC}. Considering a report from McGehee and co-workers [39] which confirms the lack of correlation between ionization

potential and V_{OC}, this result is not surprising. It has been documented that there is a reduction of work function as a consequence of the chemical reaction of PEDOT:PSS with perovskite layer at interface.[29] Therefore, the suppression of V_{OC} could well be due to the chemistry at PEDOT:PSS/perovskite interface.

The external quantum efficiency (EQE) of each device is shown in **Fig. 2b**. PEDOT:PSS device revealed a higher EQE response in the short wavelength regime (~300-400 nm). This is due to the higher absorption spectra of PTAA (**Fig. S2**). Above 400 nm, PTAA devices showed enhanced EQE response indicating improvement in perovskite thin film quality and better interface layer between perovskite and PTAA. Integrating the EQE curves estimated J_{SC} values of 19.78 and 18.21 $mAcm^{-2}$ for PTAA and PEDOT:PSS devices, respectively, which are in good agreement with the obtained J_{SC} values. The band gap energies (E_g) of the perovskite layer estimated from the EQE spectra (**Fig. S3a**) were found to be ~1.60 ± 0.01 eV for both devices. This is in agreement with the PL characteristic peaks (**Fig. S3b**).

Table 1. Device performance parameters/ properties of the PVSCs with PTAA and PEDOT:PSS as HTL. J_{SC}: short circuit current density, V_{OC}: open circuit voltage, FF: fill factor, η: power conversion efficiency, R_S: series resistance, R_{Sh}: shunt resistance, A: diode ideality factor, J_0: reverse saturation current density, *: estimated from J-V analysis and ** estimated from V_{OC}-T plot.

Device	J_{SC} (mA cm^{-2})	V_{OC} (V)	FF	η (%)	R_S ($\Omega \cdot cm^2$)	R_{Sh} ($\Omega \cdot cm^2$)	*A	*J_0 ($mAcm^{-2}$)	**E_g-E_A (eV)
With PTAA	21.01	1.09	0.79	18.07	4.79	1.52×10^4	1.07	1.12×10^{-12}	0.01
With PEDOT:PSS	19.66	0.95	0.78	14.53	4.72	2.23×10^3	1.23	3.24×10^{-11}	0.22

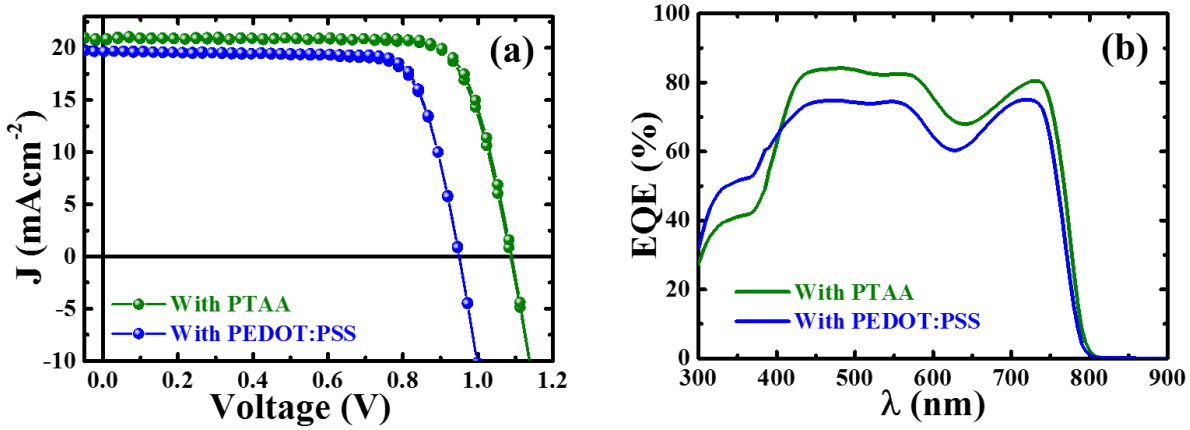

Figure 2. (a) J-V characteristics of best performing perovskite devices with PTAA and PEDOT:PSS as HTL. (b) Spectral response of corresponding devices.

Moreover, the EQE spectra of respective devices were measured under various bias voltages (**Fig. S4**). No remarkable change in EQE of each device was observed under negative bias which infers good charge collection efficiency with minimal bimolecular recombination.[6] The PTAA device revealed tolerance under various bias whereas the PEDOT:PSS device revealed significant distortion under positive bias in long wavelength regime and slight distortion in short wavelength regime. It could be due to inefficient carrier collection as consequence of stronger electrostatic stress in band alignment or local disorder due to energetic (HOMO or LUMO) offset in PEDOT:PSS device under higher positive bias.[32,40,41]

Regarding the film growth, the perovskite film on PTAA showed better film quality with larger grain size and well grown cross-sectional image compared to perovskite film on PEDOT:PSS (**Fig. S5**) as observed in other reports.[11,14] The perovskite film grown on glass/PTAA showed slightly enhanced XRD pattern (**Fig. S6**). Thus, the PTAA device with reduced grain boundaries and improved crystallinity of perovskite film grown on it has lower defect activities with decrease in non-radiative traps or deep defects.[42–44] This leads to an improvement in efficiency of PTAA device.

To get further insight, we studied the light intensity dependent V_{OC} and J_{SC} of both devices to find a clue about recombination mechanism of photogenerated charge carrier in device.[45,46] The plots of light intensity dependent J_{SC} followed a power law dependence ($J_{SC} \propto I^{\alpha}$) (**Fig. 3a**) with α~0.99 for both devices. This suggests that both devices are not limited by monomolecular recombination under short circuit.[25,45,46] A semilogarithmic plot V_{OC} as a function of light intensity (I) (**Fig. 3b**) showed a slope of 1.03 k_BT/e for PTAA device, which suggests a bimolecular recombination phenomena dominated under device operation whereas the PEDOT:PSS device resulted slightly increase in slope (1.19 k_BT/e) which indicates the occurrence of trap-assisted recombination.[45,46] In addition, the energy shift (ΔE= Eg- E_1; E_1 is intercept of V_{OC}-I plot)[30,45] is calculated to be 0.65 eV for PEDOT:PSS device which is higher than that of for PTAA device (0.57 eV). This energy shift is indicative of higher energetic disorder in device near to the interfacial layer of perovskite film and PEDOT:PSS.[10,45] Moreover, we also calculated the electrical properties of devices by analysing the J-V characteristics. [41] The results are summarized in supporting information (**Fig. S7, Table S2)**. The diode ideality factors (A) calculated from different approaches are found to be in good agreement. The values of A and J_0 are attributed to the recombination mechanism and defect activities.[47–49] The lower value of A (~1.07) for PTAA device (where, A ~1.23, for PEDOT:PSS device) suggests a reduction in recombination loss. The value of reverse saturation current density (J_0) also revealed a decreasing value from 3.24×10^{-11} $mAcm^{-2}$ for PEDOT:PSS to 1.12×10^{-12} $mAcm^{-2}$ for PTAA device. The lower values of A and J_0 for PTAA device are consistent with increase in V_{OC}. This also supports the result from the intensity dependent V_{OC}.

To explore the operating mechanism of each device, we measured the temperature dependent J-V characteristics (**Fig. S8**) in the temperature range of 233 to 353 K which is in the safe range avoiding the phase transition of perovskite crystals.[50] Although devices show

no hysteresis at room temperature, it does appear at low temperatures which is consistent with other reports.[34,51] In our PEDOT:PSS device, we observed more significant hysteresis at low temperature than what is observed for PTAA device. This enhanced hysteresis therefore suggests that the processes governing hysteresis[51–53] (such as; ion migration, surface charge accumulation, defective interface, active defect activities at low temperature) are more pronounced in PEDOT:PSS device. We note that although hysteresis is observed, J_{SC} and V_{OC} were independent of scan direction.

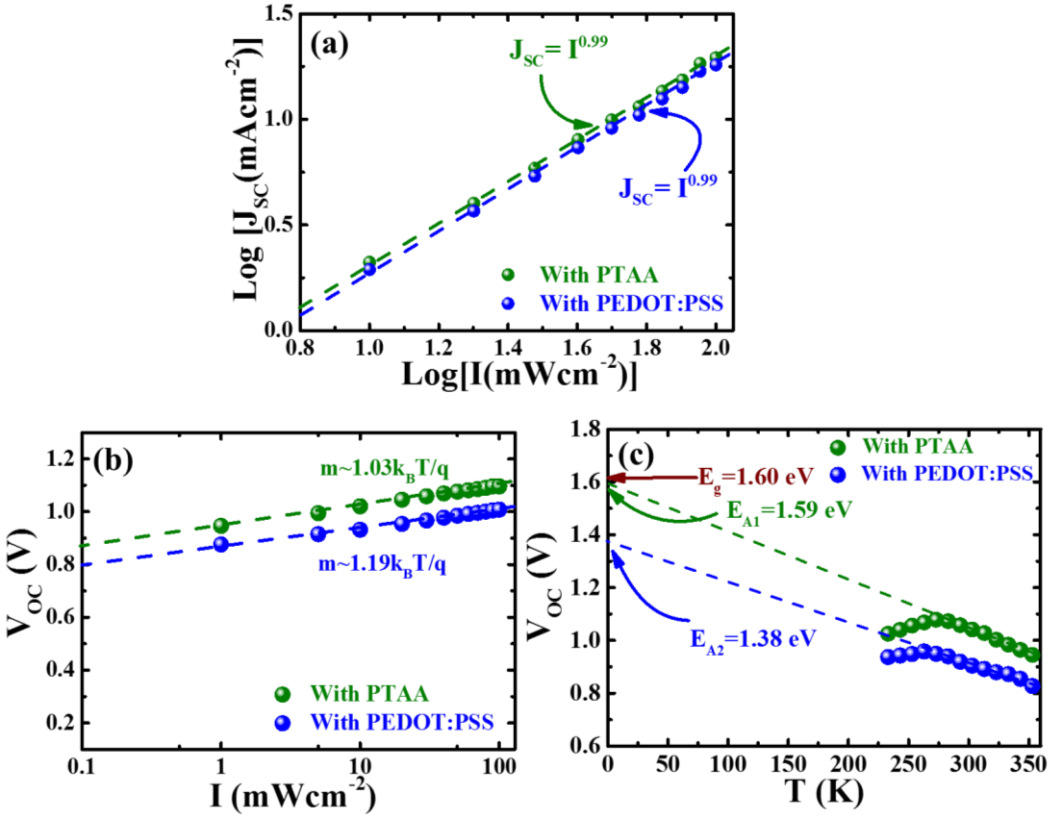

Fig. 3. Plots of light intensity dependent (I) (a) J_{SC} and (b) V_{OC} of perovskite devices with PTAA and PEDOT:PSS as HTL. Here, the dashed lines represent linear fit to respective plots. (c) Temperature dependent open circuit voltage (V_{OC}-T) of perovskite devices with PTAA and PEDOT:PSS as HTL. Here, the dashed line is linear extrapolation to T= 0 K.

The temperature dependence of V_{OC} for both devices (**Fig. 3c**) clearly shows two regimes, one above 263 K, where V_{OC} increases with decreasing temperature and a second

below 263 K, where V_{OC} decreases with temperature. Similar observations have been made for perovskite solar cells in other reports.[26,28,33] The trend of this second regime was proposed to be due to the pinning of interface or bulk defect states or that the devices being contact limited under operation at low temperatures.[28] Extrapolating the V_{OC} in the high temperature regime to T= 0 K allows us to estimate the activation energy (E_A) of dominant recombination mechanism in accordance with the relation,[41,54]

$$V_{OC} = \frac{E_A}{q} - \frac{A\,k_B T}{q} \times \ln\left(\frac{J_{00}}{J_{Ph}}\right) \qquad (1)$$

where J_{00} and J_{ph} denote reverse saturation current prefactor and photocurrent, respectively. The linear extrapolation of V_{OC}-T plots to 0 K yields E_A ~1.59 and 1.38 eV for PTAA and PEDOT:PSS devices, respectively, which are lowered (E_g-E_A) by ~ 0.01eV and ~0.22 eV from E_g of perovskite film (**Fig. S3**). The depression of E_A with respect to Eg reflects the strength of the defect-mediated recombination at the interfacial defects induced in the carrier-generating perovskite layer.[41,49,54] Note that the interface quality in device between the CTL and perovskite layer formed during device fabrication depends upon the properties of CTLs and it also affects the quality of the perovskite film grown on it.[29,43,55] The PEDOT:PSS device having higher depression of E_A indicates strong interface recombination whereas PTAA device having E_A~E_g suggests the recombination process in the bulk of perovskite layer could be more important. The results suggest that the V_{OC} in PEDOT:PSS device is limited by recombination in the defective perovskite at the PEDOT:PSS interface (we will call it as a (defective) interfacial layer, hereafter. In the numerical simulation below, we express it as a thin film distinct from the bulk perovskite and CTLs.). This could be due to hygroscopic/acidic nature of PEDOT:PSS[56–58] and its chemical reaction at interface during device fabrication.[29] Incidentally, although the band alignment is crucial for effective carrier extraction, it is reported that V_{OC} is not limited by non-optimum band alignment at

interface.[28,59] Therefore, we do not include the effect of the band alignment in discussing V_{OC} here.

All the temperature dependent device parameters are summarized in supporting information (**Fig. S9**). It is noticed that J_{SC} for PEDO:PSS device decreases with decreasing temperature whereas there is no significant impact in J_{SC} for PTAA device (**Fig. S9**). This suppression of J_{SC} can be due to the nature of highly chemically doped organic materials such as PEDOT:PSS and the defective interfacial layer under device operation at low temperature. The FF of PTAA device demonstrated a faster drop for temperature lower than 300 K. This is the consequence of increasing trend of R_S for PTAA device in the same temperature regime. Brabec and co-workers reported that the resistance of perovskite layer is not affected by temperature.[26] Therefore, the HTLs (PTAA and PEDOT:PSS) layer must be the origin of R_S trend of respective devices. Note that despite different device structures, our results showed a similar temperature dependent trend for V_{OC} as observed by Leong et al.[28] whereas the trends for J_{SC} and FF were different. It indicates that the device structures as well as CTLs/perovskite interface layer could have a significant impact on device parameters (J_{SC}, FF) under low temperature operation. The device operation with decreasing temperature can be strongly influenced by a number of factors such as the accelerated interfacial recombination, the bulk defect activities or contact limited transport. These phenomena are qualitatively studied by the capacitance spectroscopy below.

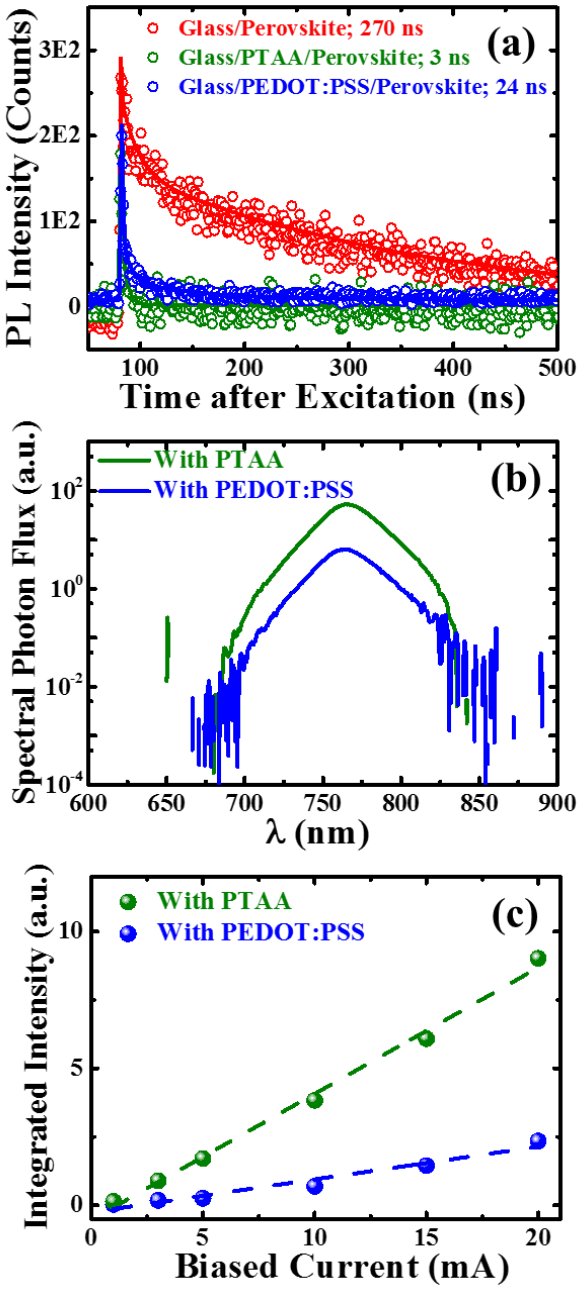

Fig. 4. Time-resolved photoluminance (TRPL) of respective films of perovskite (PVK) films, PVK/glass, PVK on PTAA and PEDOT:PSS, where PVK thin film is protected by a thin PMMA (poly(methyl methacrylate)) layer spin coating on it (a). The electroluminescence (EL) spectra of perovskite devices with PTAA and PEDOT:PSS as HTL under 5 mA biased current as a function of energy (b). The integrated EL spectra (spectral photon flux) under different applied current for respective devices (c). The dashed line represents linear fit.

To understand the HTL/perovskite interface, we measured time-resolved PL (TRPL). PL lifetimes (**Fig. 4a**) show significantly better quenching of perovskite emission by PTAA (τ = 3 ns) than by PEDOT:PSS (τ = 24 ns). The lifetime of perovskite film on bare glass is 270 ns. A short PL lifetime indicates enhanced charge transfer between perovskite and PTAA. In contrast, the electroluminescence (EL) intensity (**Fig. 4b and Fig. S10**) from PTAA device is nearly 5 fold intensified compared to that of PEDOT:PSS device under the same feeding current (~5 mA). EL is a consequence of radiative recombination of injected free carriers across the band gap. In PTAA device, the defect level is shallower (see below) and is expected to be less effective to cause the non-radiative recombination and hence the stronger EL. The normalized EL plot (**Fig. S10**) reveals that the spectral shape and energetic position do not depend on the HTLs, suggesting that the effect on the band edge of perovskite is similar in both cases.[25–27] The EL spectra with increase in the injection current (**Fig. S11**) also showed similar spectral shape for both devices. On the other hand, the integrated EL spectra (**Fig. 4c**) revealed monotonically increasing trend with injection current (I) having the slope; 0.46 and 0.12 for PTAA and PEDOT:PSS devices, respectively. The lower slope for PEDOT:PSS device signifies a stronger free carrier sink by non-radiative recombination. The results further suggest that there are comparatively higher non-radiative traps either at the interface or in the bulk for PEDOT:PSS device, which supresses the V_{OC}.

To elucidate the carrier profile and defect activities, we further investigated the devices by using capacitance spectroscopy.[60] The capacitance-voltage (C-V) scans were analyzed to extract the Mott-Schottky plot (**Fig. 5a**) and carrier distribution (**Fig. 5b**) in devices. Both devices are shown to be fully depleted, as one would expect for a p-i-n junction.[41,61,62] The plot **(Fig. 5a)** is independent of bias voltage until forward bias nears to diffusion potential (V_d)[41], beyond which depletion region collapses leading to a divergent capacitance. Here, the increase in V_d from ~0.77 to ~0.83 V as PEDOT:PSS is replaced by PTAA is consistent with

the enhancement in V_{OC}. The carrier profile of each device demonstrated almost flat distribution with minimum carrier density ~ 3×10^{15} cm^{-3} whereas the space charge region (SCR) width is found to be wider i.e. ~ 327 nm for PTAA device (294 nm for PEDOT:PSS device). The perovskite device with PTAA having SCR width comparable to thickness of perovskite film and larger V_d is beneficial for higher V_{OC} and leads to better device efficiency.

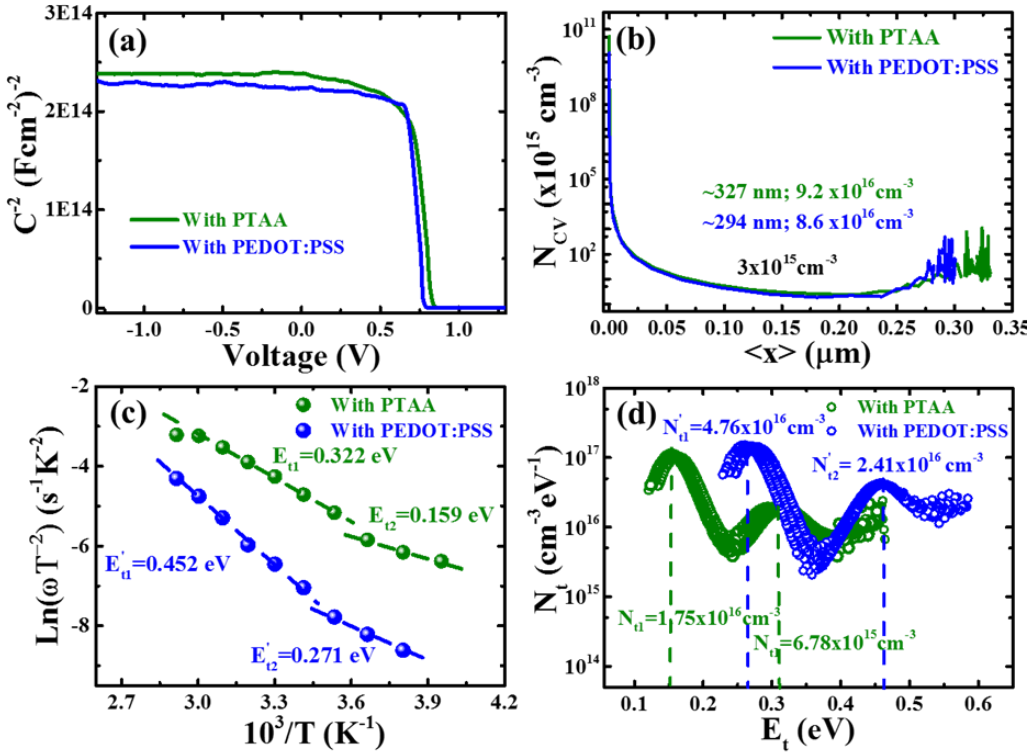

Fig. 5. Capacitance spectroscopy of perovskite devices with PTAA and PEDOT:PSS as HTL. Mott-Schottky plot (a) and carrier density profiles (b) derived from capacitance voltage (C-V) measurements. The Arrhenius plot (c) and defect distribution profile (d) of respective perovskite devices by analysing the temperature dependent capacitance-frequency (C-f-T) spectra.

Following the C-V measurements, we performed thermal capacitance spectroscopy to determine the defect level and defect density profiles of the absorber in each device.[41,54,60,63] The temperature dependent capacitance-frequency (C-f-T) scans of devices (**Fig. S12**)

showed a similar trend to our earlier report.[30] We observe a slow decrease in capacitance with temperature. The dielectric constants of the perovskite films were calculated to be ~20 and 25 from the C-f-T spectra for PTAA and PEDOT:PSS devices, respectively (**Fig. S13**) which are in the range of reported values.[64,65] **Fig. 5c** shows the Arrhenius plot extracted from the analysis of C-f-T spectra. The PEDOT:PSS device revealed two deep trap levels at E'_{t1}~ 0.452 eV and E'_{t2}~ 0.272 eV with emission factors (υ_0), 7.23×10^{10} and 2.56×10^{7} s^{-1}, respectively. The PTAA device showed shallower trap levels at E_{t1} ~0.322 eV and E_{t2}~0.159 eV with emission factors (υ'_0), 2.71×10^{9} and 2.45×10^{6} s^{-1}, respectively. Note that the both devices revealed two defect states. It is analogous to the observation of two defect states in perovskite device probed by deep level transient spectroscopy (DLTS).[66] Our results are in agreement with the reports by other groups.[15,30,65,66] Although the integrated defect densities (**Fig. 5d**) corresponding to the defect levels were found slightly lower for perovskite device with PTAA, the overall defect densities are in the range of ~10^{16} cm^{-3} for both devices, which is comparable to the reported values.[15,65,67] The CTL influence on the bulk defect level and density of defects in the perovskite film is quite understandable because the perovskite morphology depends on the CTL. Note that the location of the defects revealed by the capacitance spectroscopy cannot be assigned uniquely, in the middle or close to the interface. Furthermore, it is rather complicated to determine the origin of the defects. Tentatively, the defect states estimated in above analysis could be attributed to either iodine lead antisites (I_{Pb}), iodine interstitials (Ii) or vacancies; V_{Pb}, V_{MA} as reported from theoretical calculations.[5,68,69]

From defect analysis, the PTAA device was found to be rather effective at reducing the defect densities and mitigating deep defects. Note that the deeper defects promote Shockley Read Hall (SRH) recombination, which is detrimental to the device performance. The higher value of A for PEDOT:PSS device is in accordance with the presence of deeper traps which

indicate enhanced SRH recombination. Our results corroborate that the differences in defect activities induced in the devices with different HTLs have strong influences in device performance. Regarding the hysteresis observed in the low temperature, this correlates well with the emission factors recorded for each device. The more exaggerated hysteresis of PEDOT:PSS device may originate from dominant capturing and emitting tendency of either the active defect levels in bulk and recombination in the defective interfacial layer at low temperature.

To have a deeper understanding on the influence of HTLs on device performance, device simulation was carried out using the program SCAPS (ver. 3.3.01),[58] solar cell capacitance simulator adopting the device layers shown in **Fig. S14a** resembling the real device with the layer properties (**Table S3**) defined with the reference of our earlier report.[30] This tool has some degrees of freedom to define the layer properties and film quality to mimic the experimental results.[71,72] We performed the device simulation considering the experimental results with account of the bulk material quality (defect level, defect density) and the defective interfacial layer quality induced in device with HTLs; PEDOT:PSS and PTAA. The simulated energy band diagram is as depicted in **Fig. S14b**. The simulated J-V characteristics as depicted in **Fig. S15** and **Table S3** demonstrate a good agreement with the general feature of experimental results. The simulation results showed lower recombination current density and recombination carrier density (**Fig. S16**) for PTAA device. If we have a close look, the recombination rates (**Fig. S16b**) either at interface and bulk of perovskite layer are quite higher for PEDOT:PSS device. Furthermore, we also performed simulation considering the bulk/interface defect states and densities to account for the different contributions from the perovskite film and interfacial layer quality as shown in **Fig. S17**. The simulation indicates that the bulk defects affect J_{SC} more while the interfacial defects are more influential on Voc. The latter is consistent with the conventional interpretation of **Fig. 3**

C above. Both factors combined together determine the total PCE. Although we cannot determine quantitatively the relative importance of the two, it is clear that one mechanism does not dominate over the other here; both are equally important.

The comparative studies on device characteristics by experimental and simulation approach corroborate that the PTAA device effectively suppresses bulk defect activities and interface recombination phenomena leading to better device performance. Thus, one can expect further progress in device performance by improving the quality of HTLs in terms of the passivation of interface recombination and the reduction of grain boundaries in perovskite films.

Conclusions

We systematically studied the impacts of charge transport layers on performance of perovskite devices focusing the effect on optoelectronic properties. The analysis of J-V characteristics, optophysical properties and capacitance spectra of devices revealed improvement in interface quality, efficient carrier transport and mitigation of defect levels in perovskite device with PTAA as HTL. PEDOT:PSS device found to be limited from dominant interface recombination with a lower activation energy of interfacial recombination (E_A~1.38 eV< Eg~1.60 eV) and deep defects (Et~ 0.271 and 0.452 eV) in perovskite layer. Our results infer passivation of recombination activities and better interface quality in PTAA device. It leads to an enhancement in power conversion efficiency to ~18.1% (14.5% for PEDOT:PSS device). This work corroborates that the selection of HTLs is crucial for further enhancement in device performance.

Experimental section

Materials and preparation

All chemicals were purchased from commercial suppliers as mentioned and unless otherwise specified, they were used as received. For the fabrication of perovskite films, precursor solutions were prepared by dissolving PbI_2 [Kanto-chemical, 98% purity] in anhydrous DMF (500 mg ml^{-1}) and methyl ammonium iodide (MAI) + methyl ammonium chloride (MACl) [Wako Chemicals, battery grade] in ethanol (50 mg ml^{-1}; 19:1 ratio). Poly [bis(4-phenyl)(2,4,6-trimethylphenyl)amine (PTAA) [Sigma Aldrich, 99% purity] solution (0.5 wt. %) dissolved in anhydrous chlorobenzene (CB) was used for coating of the hole transport layer (HTL). [6,6]-Phenyl C_{61} butyric acid methyl ester ($PC_{61}BM$) [Sigma Aldrich, 99% purity] solution (2 wt. %) dissolved in anhydrous chlorobenzene (CB) was used for coating of the electron transport layer (ETL). All the solutions were filtered using 0.45 μm syringe filters to avoid the risk of unwanted particles in the precursor solution. Aluminium doped zinc oxide (AZO) nanoparticle ink (Nanograde N-21X) was used to prepare AZO layer.

Device Fabrication

Solar cell devices were fabricated on pre-cleaned patterned indium tin oxide (ITO) coated glass substrates (15 Ω $square^{-1}$). The ITO substrates were pre-cleaned in an ultrasonic bath with detergent, pure water, and 2-propanol, followed by an ultraviolet-ozone treatment for 5 min to remove the organic residuals. We have prepared perovskite device with two kind of HTM layers. A thin HTM layer (20 nm) of PTAA was deposited onto ITO substrate by spin coating at 1000 rpm and subsequently dried at 100 ℃ for 5 min on a hot plate in nitrogen ambient. Similarly another thin HTM layer (30 nm) of poly(3,4-ethylenedioxythiophene):poly(styrene sulfonate) (PEDOT:PSS, Clevios, Al4083)

was deposited onto ITO substrate by spin coating at 3000 rpm and subsequently dried at 130 ℃ for 10 min on a hot plate in air ambient. Then substrates were transferred into a nitrogen-filled glove box (<1.0 ppm O_2 and H_2O) and the rest of the steps were carried out inside the glove box. PbI_2 precursor solution was spin coated at 3000 rpm for 90 s and a mixed precursor solution of MAI + MACl was subsequently spun on to the PbI_2 layer at 4000 rpm, for 30 s. Then to promote the crystallization, those as grown $CH_3NH_3PbI_{3-x}Cl_x$ perovskite films were simply placed on hot plate with MACl powder covered with petri dish at 100 ℃.[20,30] For ETM layer, $PC_{61}BM$ was spun–coated on top of the perovskite films at 700 rpm for 30 s coupled at 5000 rpm for 10 s, followed by deposition of a thin AZO layer spinning at 2500 rpm for 25 s. To complete device structure, samples were then transferred into the evaporation chamber connected to the glove box for metal contact deposition. Finally, 100 nm of Ag was thermally evaporated at a pressure $<10^{-4}$ Pa. Devices with area of ~0.26 cm^2 were sealed using UV-curable resins before the subsequent measurements in ambient conditions.

Characterization

The X-ray diffraction (XRD) patterns of fabricated perovskite films were measured using Bruker D8 advanced x-ray diffractometer (CuK_α radiation, λ= 1.54050 A). The morphology of films and cross-sectional images were taken by a high resolution scanning electron microscope (SEM) at 5 kV accelerating voltage (Hitachi, S-4800). The absorption spectra and photoluminescence (PL) spectra of various films were taken using UV-Vis-NIR spectrometer (7200, V-Jasco) and Spectrofluorometer (FP8500, Jasco). HOMO levels of ETLs, HTLs and PVK and the work functions of ITO and Ag were measured with a photoelectron spectrometer (Riken Keiki, AC-3). The carrier life times were measured with a fluorescence lifetime spectrometer (Quantaurus- τ from Hamamatsu- Photonics K.K.). Electroluminescence (EL) spectra of devices were performed under biased current supplied

by an external current/voltage source through the devices. The emitted light then collected by Si CCD array detector from Horiba. The current density–voltage (J-V) characteristics and spectral response (incident monochromatic photon to current conversion efficiency (IPCE) spectra, external quantum efficiency (EQE), and reflectance spectra) were characterized with a spectrometer (SM-250IQE, Bunkokeiki, Japan). Capacitance-frequency response (C-f) was measured with an LCR meter (E4980A, Agilent), which probes from 20 Hz to 2 MHz at ac voltage amplitude of 10 mV under dark condition in the temperature range of 253 K−343 K whereas capacitance-voltage (C−V) measurements were carried out at 5 kHz. For temperature dependent C−f scans and J-V characteristics, a temperature controlled chamber (SU-221) was used having control system with error of ±0.1 K (℃).

Supporting information

The supporting information is available free of charge on RSC Publications website.
Experimental methods and additional figures and tables.

Notes

The authors declare no competing financial interest.

Acknowledgements

The authors acknowledge the support under the MEXT Program for Development of Environment Technology using Nanotechnology (GREEN), JSPS KAKENHI grant number JP16K06285

References

1 M. M. Lee, J. Teuscher, T. Miyasaka, T. N. Murakami and H. J. Snaith, *Science*, 2012, **338**, 643–647.

2 H. Kim, C.-R. Lee, J. Im, K. Lee, T. Moehl, A. Marchioro, S. Moon, R. Humphry-Baker, J. Yum, J. E. Moser, M. Grätzel and N.-G. Park, *Sci. Rep.*, 2012, **2**, 591.

3 M. A. Green, K. Emery, Y. Hishikawa, W. Warta, E. D. Dunlop, D. H. Levi and A. W. Y. Ho-baillie, *Prog. Photovolt Res. Appl.*, 2017, **25**, 3–13.

4 T. M. Brenner, D. A. Egger, L. Kronik, G. Hodes and D. Cahen, *Nat. Rev. Mater.*, 2016, **1**, 15007.

5 Y. Y. and S.-H. W. Wan-Jian Yin, Ji-Hui Yang Joongoo Kang, *J. Mater. Chem. A*, 2015, **3**, 8926–8942.

6 Q. Lin, A. Armin, R. Chandra, R. Nagiri, P. L. Burn and P. Meredith, *Nat. Photonics*, 2014, **9**, 106–112.

7 J. Burschka, N. Pellet, S.-J. Moon, R. Humphry-Baker, P. Gao, M. K. Nazeeruddin and M. Grätzel, *Nature*, 2013, **499**, 316–320.

8 N. J. Jeon, J. H. Noh, Y. C. Kim, W. S. Yang, S. Ryu and S. Il Seok, *Nat. Mater.*, 2014, **13**, 897–903.

9 Y. Deng, Q. Dong, C. Bi, Y. Yuan and J. Huang, *Adv. Energy Mater.*, 2016, 1600372.

10 S. Yuchuan, Y. Yuan and H. Jinsong, *Nat. Energy*, 2016, **1**, 15001.

11 C. Bi, Q. Wang, Y. Shao, Y. Yuan, Z. Xiao and J. Huang, *Nat. Commun.*, 2015, **6**, 7747.

12 C. Chueh, C. Li and A. K. Jen, *Energy Environ. Sci.*, 2015, **8**, 1160–1189.

13 J. You, L. Meng, T.-B. Song, T.-F. Guo, Y. (Michael) Yang, W.-H. Chang, Z. Hong, H. Chen, H. Zhou, Q. Chen, Y. Liu, N. De Marco and Y. Yang, *Nat. Nanotechnol.*, 2016,

11, 75–82.

14 M. Hu, C. Bi, Y. Yuan, Y. Bai and J. Huang, *Adv. Sci.*, 2015, **3**, 1500301.

15 Y. Shao, Z. Xiao, C. Bi, Y. Yuan and J. Huang, *Nat. Commun.*, 2014, **5**, 5784.

16 K. Miyano, M. Yanagida, N. Tripathi and Y. Shirai, *J. Phys. Chem. Lett.*, 2016, **7**, 2240−2245.

17 J. H. Heo, S. H. Im, J. H. Noh, T. N. Mandal, C. Lim, J. A. Chang, Y. H. Lee, H. Kim, A. Sarkar, K. NazeeruddinMd, M. Gratzel and S. Il Seok, *Nat Phot.*, 2013, **7**, 486–491.

18 S. Ryu, J. H. Noh, N. J. Jeon, Y. C. Kim, W. S. Yang, J. Seo and S. Il Seok, *Energy Environ. Sci.*, 2014, **7**, 2614–2618.

19 N. Arora, S. Orlandi, M. I. Dar, S. Aghazada, G. Jacopin, M. Cavazzini, E. Mosconi, P. Gratia, F. De Angelis, G. Pozzi, M. Graetzel and M. K. Nazeeruddin, *ACS Energy Lett.*, 2016, **1**, 107–112.

20 N. Tripathi, M. Yanagida, Y. Shirai, T. Masuda, L. Han, K. Miyano, J. Mater, A. Chem, N. Tripathi, M. Yanagida, Y. Shirai, T. Masuda, L. Han and K. Miyano, *J. Mater. Chem. A*, 2015, **3**, 12081–12088.

21 P. Calado, A. M. Telford, D. Bryant, X. Li, J. Nelson, B. C. O'Regan and P. R. F. Barnes, *Nat Commun*, 2016, **7**, 13831.

22 R. A. Belisle, W. H. Nguyen, A. R. Bowring, P. Calado, X. Li, S. J. C. Irvine, M. D. McGehee, P. R. F. Barnes and B. C. O'Regan, *Energy Environ. Sci.*, 2017, **131**, 6050.

23 W. Tress, N. Marinova, T. Moehl, S. M. Zakeeruddin, N. Mohammad K., M. Grätzel, M. K. Nazeeruddin and M. Grätzel, *Energy Environ. Sci.*, 2015, **8**, 995–1004.

24 A. M. A. Leguy, J. M. Frost, A. P. McMahon, V. G. Sakai, W. Kochelmann, C. Law,

X. Li, F. Foglia, A. Walsh, B. C. O'Regan, J. Nelson, J. T. Cabral and P. R. F. Barnes, *Nat. Commun.*, 2015, **6**, 7124.

25 Y. Hou, W. Chen, D. Baran, T. Stubhan, N. A. Luechinger, B. Hartmeier, M. Richter, J. Min, S. Chen, C. Omar, R. Quiroz, N. Li, H. Zhang, T. Heumueller, G. J. Matt, A. Osvet, K. Forberich, Z. Zhang, Y. Li, B. Winter, P. Schweizer, E. Spiecker and C. J. Brabec, *Adv. Mater.*, 2016, **28**, 5112–5120.

26 S. Chen, Y. Hou, H. Chen, M. Richter, F. Guo, S. Kahmann, X. Tang, T. Stubhan, H. Zhang, N. Li, N. Gasparini, C. O. R. Quiroz, L. S. Khanzada, G. J. Matt, A. Osvet and C. J. Brabec, *Adv. Energy Mater.*, 2016, 1600132.

27 J. Yao, T. Kirchartz, M. S. Vezie, M. A. Faist, W. Gong, Z. He, H. Wu, J. Troughton, T. Watson, D. Bryant and J. Nelson, *Phys. Rev. Appl.*, 2015, **4**, 14020.

28 W. L. Leong, Z. Ooi, D. Sabba, C. Yi, S. M. Zakeeruddin, M. Graetzel, J. M. Gordon, E. A. Katz and N. Mathews, *Adv. Mater.*, 2016, **28**, 2439–2445.

29 T. Liu, F. Jiang, F. Qin, W. Meng, Y. Jiang, S. Xiong, J. Tong, Z. Li, Y. Liu and Y. Zhou, *ACS Appl. Mater. Interfaces*, 2016, **8**, 33899−33906.

30 D. B. Khadka, Y. Shirai, M. Yanagida, T. Masuda and K. Miyano, *Suataintable Energy and Fuels*, 2017, **1**, 755–766.

31 X. Xu, C. Ma, Y. Cheng, Y. M. Xie, X. Yi, B. Gautam, S. Chen, H. W. Li, C. S. Lee, F. So and S. W. Tsang, *J. Power Sources*, 2017, **360**, 157–165.

32 R. Cao, F. Xu, J. Zhu, S. Ge, W. Wang, H. Xu, R. Xu, Y. Wu, Z. Ma, F. Hong and Z. Jiang, *Adv. Energy Mater.*, 2016, 1600814.

33 L. Cojocaru, S. Uchida, Y. Sanehira, G.-P. Victoria, B. Juan, N. Jotaro, K. Takaya and H. Segawa, *Chem. Lett.*, 2015, **44**, 1557–1559.

34 L. K. Ono, S. R. Raga, S. Wang, Y. Kato and Y. Qi, *J. Mater. Chem. A*, 2015, **3**, 9074–9080.

35 H. Zhang, X. Qiao, Y. Shen, T. Moehl, S. M. Zakeeruddin and M. Wang, *J. Mater. Chem. A*, 2015, **3**, 11762–11767.

36 N. Tripathi, Y. Shirai, M. Yanagida, A. Karen and K. Miyano, *ACS Appl. Mater. Interfaces*, 2016, **8**, 4644–4650.

37 K. A. Bush, C. D. Bailie, Y. Chen, T. Leijtens, A. R. Bowring, F. Moghadam and M. D. McGehee, *Adv. Mater. Submitt.*, 2015, **28**, 1–7.

38 A. Savva, I. Burgués-Ceballos and S. A. Choulis, *Adv. Energy Mater.*, 2016, **6**, 1600285.

39 R. A. Belisle, P. Jain, R. Prasanna, T. Leijtens and M. D. McGehee, *ACS Energy Lett.*, 2016, **1**, 556–560.

40 A. Armin, I. Kassal, P. E. Shaw, M. Hambsch, M. Stolterfoht, D. M. Lyons, J. Li, Z. Shi, P. L. Burn and P. Meredith, *J. Am. Chem. Soc.*, 2014, **136**, 11465–11472.

41 S. S. Hegedus and W. N. Shafarman, *Prog. Photovoltaics Res. Appl.*, 2004, **12**, 155–176.

42 A. Sharenko and M. F. Toney, *J. Am. Chem. Soc.*, 2016, **138**, 463–470.

43 W. Zhang, S. Pathak, N. Sakai, T. Stergiopoulos, P. K. Nayak, N. K. Noel, A. A. Haghighirad, V. M. Burlakov, D. W. DeQuilettes, A. Sadhanala, W. Li, L. Wang, D. S. Ginger, R. H. Friend and H. J. Snaith, *Nat. Commun.*, 2015, **6**, 10030.

44 W. Nie, H. Tsai, R. Asadpour, A. J. Neukirch, G. Gupta, J. J. Crochet, M. Chhowalla, S. Tretiak, M. A. Alam and H. Wang, 2015, **347**, 522–526.

45 S. R. Cowan, A. Roy and A. J. Heeger, *Phys. Rev. B*, 2010, **82**, 245207.

46 X. Du, O. Lytken, M. S. Killian, J. Cao, T. Stubhan, M. Turbiez, P. Schmuki, H. P. Steinruck, L. Ding, R. H. Fink, N. Li and C. J. Brabec, *Adv. Energy Mater.*, 2016, 1601959.

47 D. Song, J. Ji, Y. Li, G. Li, M. Li, T. Wang, D. Wei, P. Cui, Y. He and J. M. Mbengue, *Appl. Phys. Lett.*, 2016, **108**, 93901.

48 D. B. Khadka, S. Kim and J. Kim, *J. Phys. Chem. C*, 2016, **120**, 4251–4258.

49 V. Nadenau, U. Rau, A. Jasenek and H. Schock, *J. Appl. Phys.*, 2000, **87**, 584.

50 A. Poglitsch and D. Weber, *J. Chem. Phys.*, 1987, **87**, 6373–6378.

51 D. Bryant, S. Wheeler, B. C. O'Regan, T. Watson, P. R. F. Barnes, D. Worsley and J. Durrant, *J. Phys. Chem. Lett.*, 2015, **6**, 3190–3194.

52 H. J. Snaith, A. Abate, J. M. Ball, G. E. Eperon, T. Leijtens, N. K. Noel, S. D. Stranks, J. T. W. Wang, K. Wojciechowski and W. Zhang, *J. Phys. Chem. Lett.*, 2014, **5**, 1511–1515.

53 B. Chen, M. Yang, S. Priya and K. Zhu, *J. Phys. Chem. Lett.*, 2016, **7**, 905–917.

54 D. B. Khadka, S. Kim and J. Kim, *J. Phys. Chem. C*, 2015, **119**, 12226–12235.

55 J. Liu, C. Gao, X. He, Q. Ye, L. Ouyang, D. Zhuang, C. Liao, J. Mei and W. Lau, *ACS Appl. Mater. Interfaces*, 2015, **7**, 24008–24015.

56 W. Lee, M. Song, S. Park, S. Nam, J. Seo, H. Kim and Y. Kim, *Sci. Rep.*, 2016, **6**, 33795.

57 L. Meng, J. You, T.-F. Guo and Y. Yang, *Acc. Chem. Res.*, 2016, **49**, 155–165.

58 Q. Wang, C.-C. Chueh, M. Eslamian and A. K.-Y. Jen, *ACS Appl. Mater. Interfaces*,

2016, **8**, 32068–32076.

59 P. Schulz, E. Edri, S. Kirmayer, G. Hodes, D. Cahen and A. Kahn, *Energy Environ. Sci.*, 2014.

60 D. Abou-Ras, T. Kirchartz and U. Rau, *Advanced Characterization Techniques for Thin Film Solar Cells*, Wiley-VCH Verlag GmbH & Co. KGaA: Weinheim, Germany, 2016.

61 H. Tsai, W. Nie, J. Blancon, C. C. Stoumpos, R. Asadpour, B. Harutyunyan, A. J. Neukirch, R. Verduzco, J. J. Crochet, S. Tretiak, L. Pedesseau, J. Even, M. A. Alam, G. Gupta, J. Lou, P. M. Ajayan, M. J. Bedzyk, M. G. Kanatzidis and A. D. Mohite, 2016, **356**, 312–316.

62 O. Almora, C. Aranda, E. Mas-Marz and Garcia-Belmonte, *Appl. Phys. Lett.*, 2016, **109**, 173903.

63 T. Walter, R. Herberholz, C. Müller and H. W. Schock, *J. Appl. Phys.*, 1996, **80**, 4411–4420.

64 O. Almora, I. Zarazua, E. Mas-marza, I. Mora-sero, J. Bisquert and G. Garcia-belmonte, *J. Phys. Chem. Lett.*, 2015, **6**, 1645−1652.

65 H. Duan, H. Zhou, Q. Chen, P. Sun, S. Luo, T. Song, B. Bob and Y. Yang, *Phys. Chem. Chem. Phys.*, 2015, **17**, 112–116.

66 S. Heo, G. Seo, Y. H. Lee, D. Lee, M. Seol, J. Lee, J.-B. Park, K. Kim, D.-J. Yun, Y. Kim, J. Shin, T. K. Ahn and M. K. Nazeeruddin, *Energy Environ. Sci.*, 2017, 0–6.

67 J. H. Heo, D. H. Song, H. J. Han, S. Y. Kim, J. H. Kim, D. Kim, H. W. Shin, T. K. Ahn, C. Wolf, T. W. Lee and S. H. Im, *Adv. Mater.*, 2015, **27**, 3424–3430.

68 J. M. Azpiroz, E. Mosconi, J. Bisquert and F. De Angelis, *Energy Environ. Sci.*, 2015, **8**, 2118–2127.

69 M. H. Du, *J. Mater. Chem. A*, 2014, **2**, 9091–9098.

70 M. Burgelman, P. Nollet and S. Degrave, *Thin Solid Films*, 2000, **361**, 527–532.

71 J. Pettersson, M. Edoff and C. Platzer-Björkman, *J. Appl. Phys.*, 2012, **111**, 14509.

72 F. Pianezzi, P. Reinhard, A. Chirilă, S. Nishiwaki, B. Bissig, S. Buecheler and A. N. Tiwari, *J. Appl. Phys.*, 2013, **114**, 1945081.

Table of Contents Graphics

The performance of perovskite device was found to be influenced by the interface quality and bulk defect activities induced in perovskite grown on HTL during device fabrication.